Comitato Nazionale per l'Energia Nucleare
ISTITUTO NAZIONALE DI FISICA NUCLEARE

INFN/BE - 66/12
20 Dicembre 1966

R. Giacomich, L. Granata and F. de Guarrini:

FAST NEUTRON SPECTROSCOPY WITH TIME-OF-FLIGHT AND ASSOCIATED PARTICLE METHOD

Servizio riproduzione della
Sottosezione di Trieste dell'INFN

FAST NEUTRON SPECTROSCOPY WITH TIME-OF-FLIGHT AND ASSOCIATED PARTICLE METHOD (*)

R. Giacomich, L. Granata and F. de Guarrini

Istituto di Fisica dell'Università - Trieste

Istituto Nazionale di Fisica Nucleare - Sottosezione di Trieste

(*) Work performed under Contract EURATOM-CNEN

1. - INTRODUCTION

The spectroscopy of neutrons elastically and inelastically scattered by nuclei is a very valuable tool for obtaining useful information concerning the scattering mechanism, the nuclear level density and the various features of the nuclear models [1-10].

The object of this type of experiments consists in measuring the energy of the neutrons scattered by the target nucleus. This is achieved with the time of flight method by measuring the time t required for the neutron to cover a given distance ℓ : the neutron energy E is then derived using the formula

$$(1) \qquad t = \frac{72.3}{\sqrt{E}} \, \ell \, ,$$

where t is expressed in nsec, E in MeV, ℓ in meters. Because of various reason to be discussed below, the time t is determined with an uncertainty Δt consequently the energy E will be known with an error ΔE related to Δt by the equation

$$(2) \qquad \frac{\Delta E}{E} = 2 \, \frac{\Delta t}{t}$$

The ratio $\frac{\Delta E}{E}$ gives the energy resolution of the experimental apparatus.

When a certain nucleus is to be studied, the problem raises to design the time of flight equipment so to be able to resolve the neutrons scattered from the different levels of the target nucleus. Therefore, the various terms contributing to the time uncertainty Δt have to be carefully estimated and provision has to be made in order to keep $\frac{\Delta t}{t}$, and hence $\frac{\Delta E}{E}$, within limits allowing a clear separation of the neutron energies. Of course, in so doing one may finally be facing limitations that can not be overcome by no means.

The quantity Δt may be regarded as the resultant of two terms assumed to have independent gaussian distributions, that is,

$$\Delta t^2 = \Delta t_1^2 + \Delta t_2^2 \, . \tag{3}$$

Δt_1 is due to the fact that one does not know the exact point within the finite lenght $\Delta \ell$ of the detector where the neutron is detected, and is related to $\Delta \ell$ by

$$\Delta t_1 = \frac{\Delta \ell}{v}$$

being v the neutron velocity.

Δt_2 takes into account all the other time uncertainties due to the electronics, to the source characteristics and so on.

One can then write

$$\Delta t = \sqrt{\left(\frac{\Delta \ell}{v}\right)^2 + (\Delta t_2)^2}$$

and

$$\frac{\Delta t}{t} = \frac{v\Delta t}{\ell} = \frac{v}{\ell}\sqrt{\left(\frac{\Delta \ell}{v}\right)^2 + (\Delta t_2)^2} = \frac{\sqrt{(\Delta \ell)^2 + (v\Delta t_2)^2}}{\ell} \, .$$

One has finally

$$\frac{\Delta E}{E} = 2\,\frac{\sqrt{(\Delta \ell)^2 + (v\Delta t_2)^2}}{\ell} \, . \tag{4}$$

One can see from Eq. (4) that in principle the precision of the time of flight measurements can be made arbitrarily high by increasing the distance ℓ over which the time is measured.

Figures 1 and 2 show the dependence between the quantities contained in Eq. (4) and can be used to solve pratical problems.

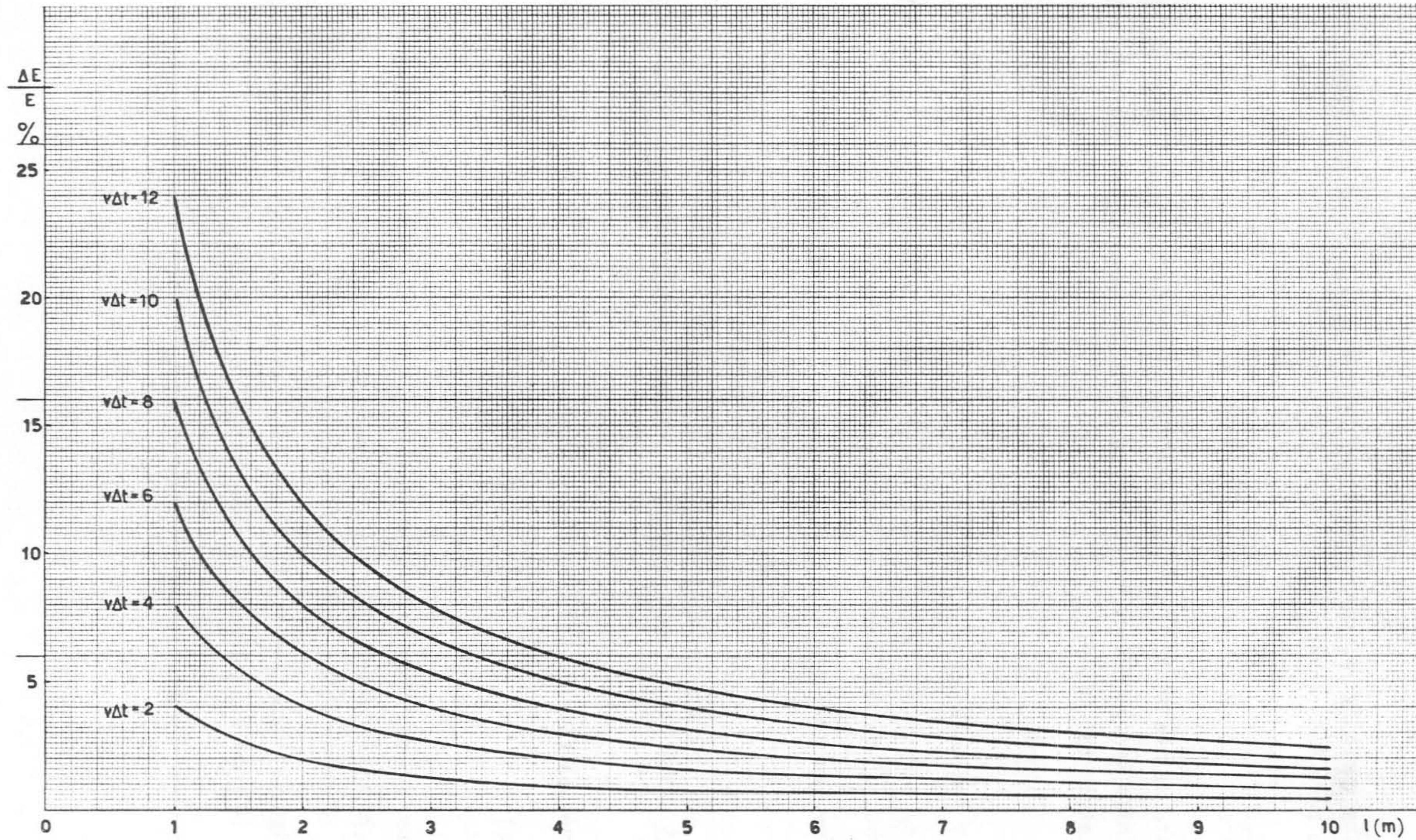

Fig. 1 - Variation of $\Delta E/E$ with $\underline{\ell}$ for different values of the parameter $v\Delta t = \sqrt{(\Delta\ell)^2 + (v\Delta t_2)^2}$ and for a neutron energy of 14.2 MeV.

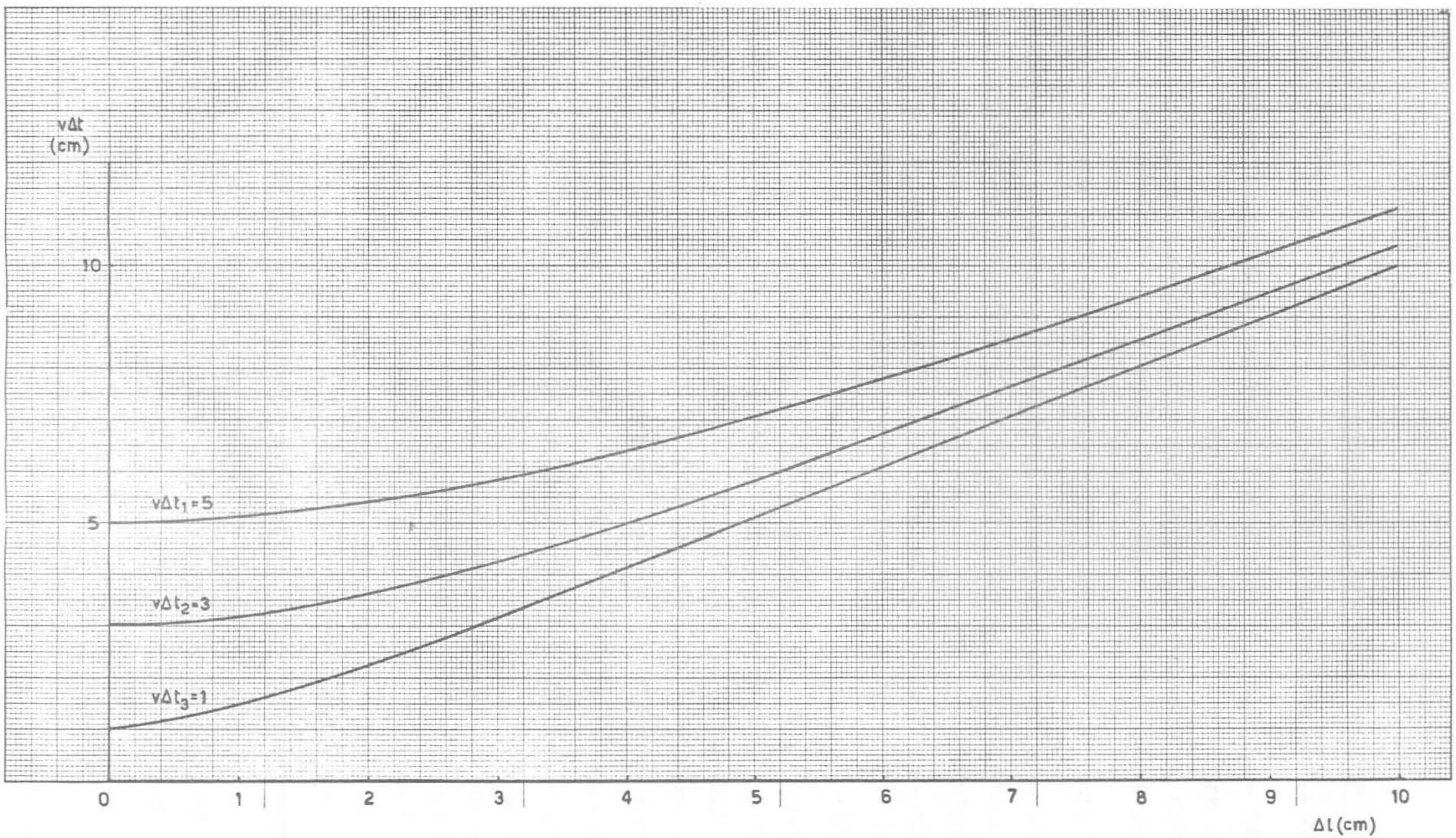

Fig. 2 - Variation of $v\Delta t = \sqrt{(\Delta\ell)^2 + (v\Delta t_2)^2}$ with $\Delta\ell$ for different values of the parameter $v\Delta t_2$ and for a neutron energy of 14 MeV.

2. - THE TIME OF FLIGHT APPARATUS USED AT THE ISTITUTO DI FISICA DI TRIESTE

The experiments of elastic and inelastic scattering of neutrons by nuclei, with the time of flight method, are carried out at the Istituto di Fisica di Trieste using the 14 MeV neutrons produced with a 600 keV Cockroft-Walton and the reaction $T(d,n)He^4$.

A block diagram of the time of flight apparatus is shown in Fig. 3.

The zero for the time scale is obtained by means of the so called "associated particle method", that is by detecting the α -particle emitted simultaneously with the neutron in the production reaction. The α-particle is detected by means of a scintillator NE 102 A, 0.1 mm. thick, coupled with a 56 AVP photomultiplier through a 3 mm. thick light pipe. (Fig. 4).

The neutrons are detected at the end of their flight path by means of a 2" × 3" liquid scintillator NE 213 coupled with a 56 AVP photomultipler. Alternatively, either a 2" × 1.5" NE 102 A plastic scintillator coupled with a 56 AVP phototube or a 4" × 1" NE 102 A scintillator coupled with a phototube XP 1040 have been used.

For environmental and shielding reasons, the requisite of detecting neutrons scattered at different angles has been met by allowing the α-detector to rotate toghether with the scatterer around the deuteron beam direction[11,12]. In fact, had the neutron detector been allowed to rotate around the scatterer, the flight path could not have been made longer than 1.5 meters due to impediment existing in the experimental room. Moreover, a fixed positioning of the n-detector allows to arbitrarly augment the shield.

The electronic chain consists of a "fast-slow" system. The fast signal is taken from the anode of the phototube, the slow signal from the 14 dinode by means of the circuit shown in Fig. 5. The voltage divider is of the B type, suggested by the manufacturer.

The neutron fast channel consists of a shaping circuit, whose operation is based on the characteristics of a tunnel diode, and of a Hewlett Packard, type A, wide band amplifier.

BLOCK SCHEME WITH THE NEUTRON SOURCE

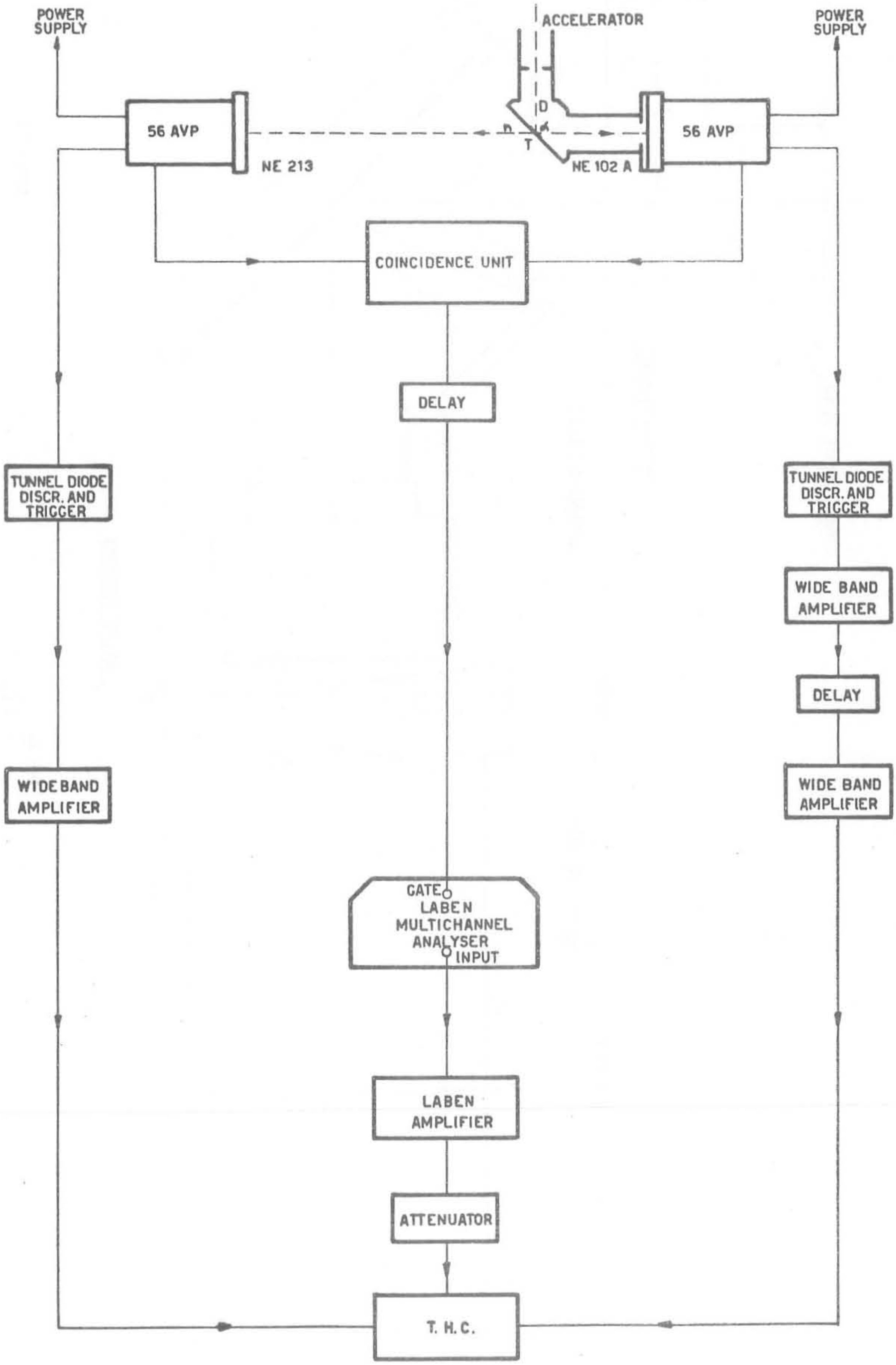

Fig. 3

ALPHA CHANNEL ASSEMBLY WITH THE NEUTRON SOURCE

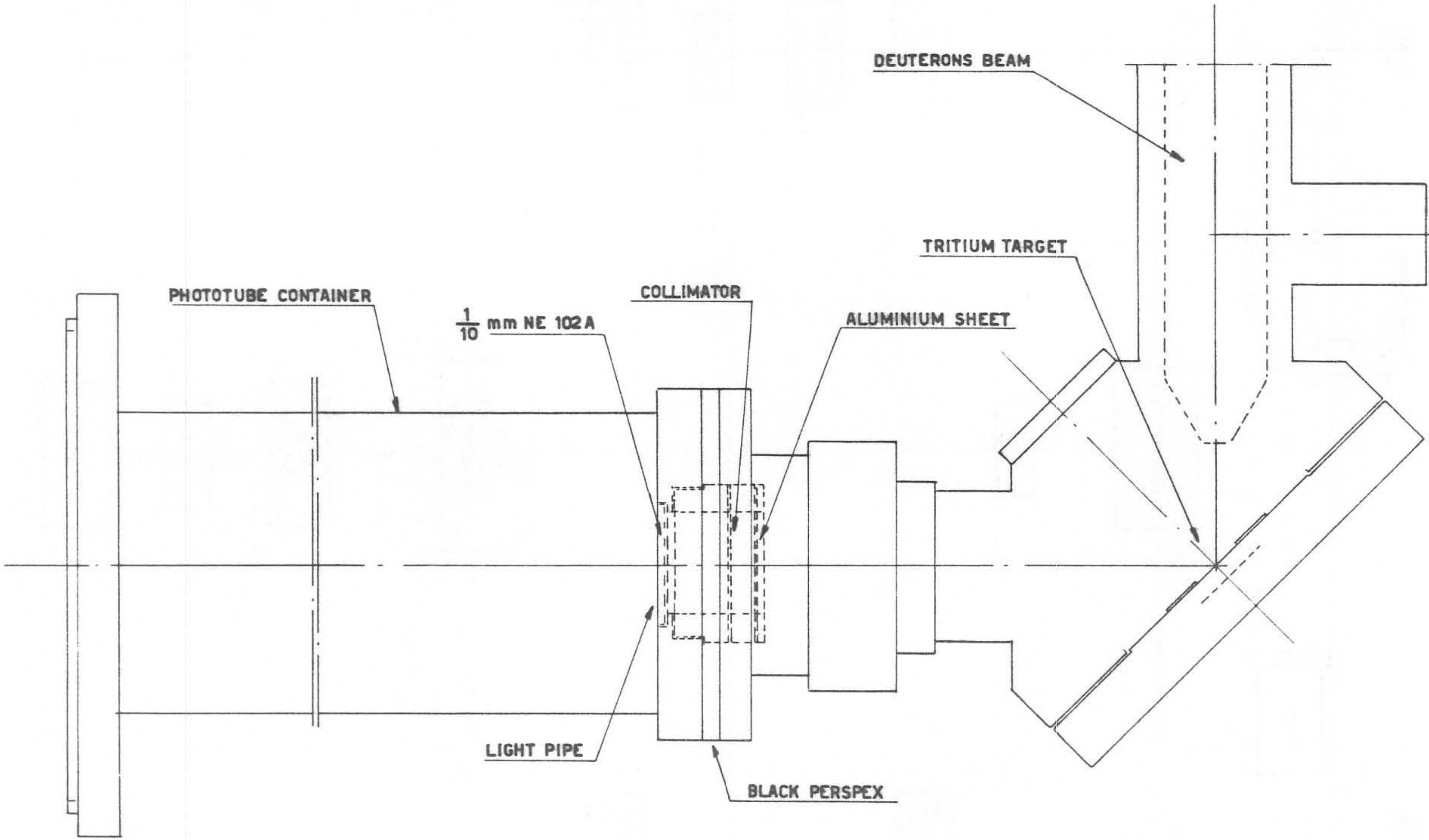

Fig. 4

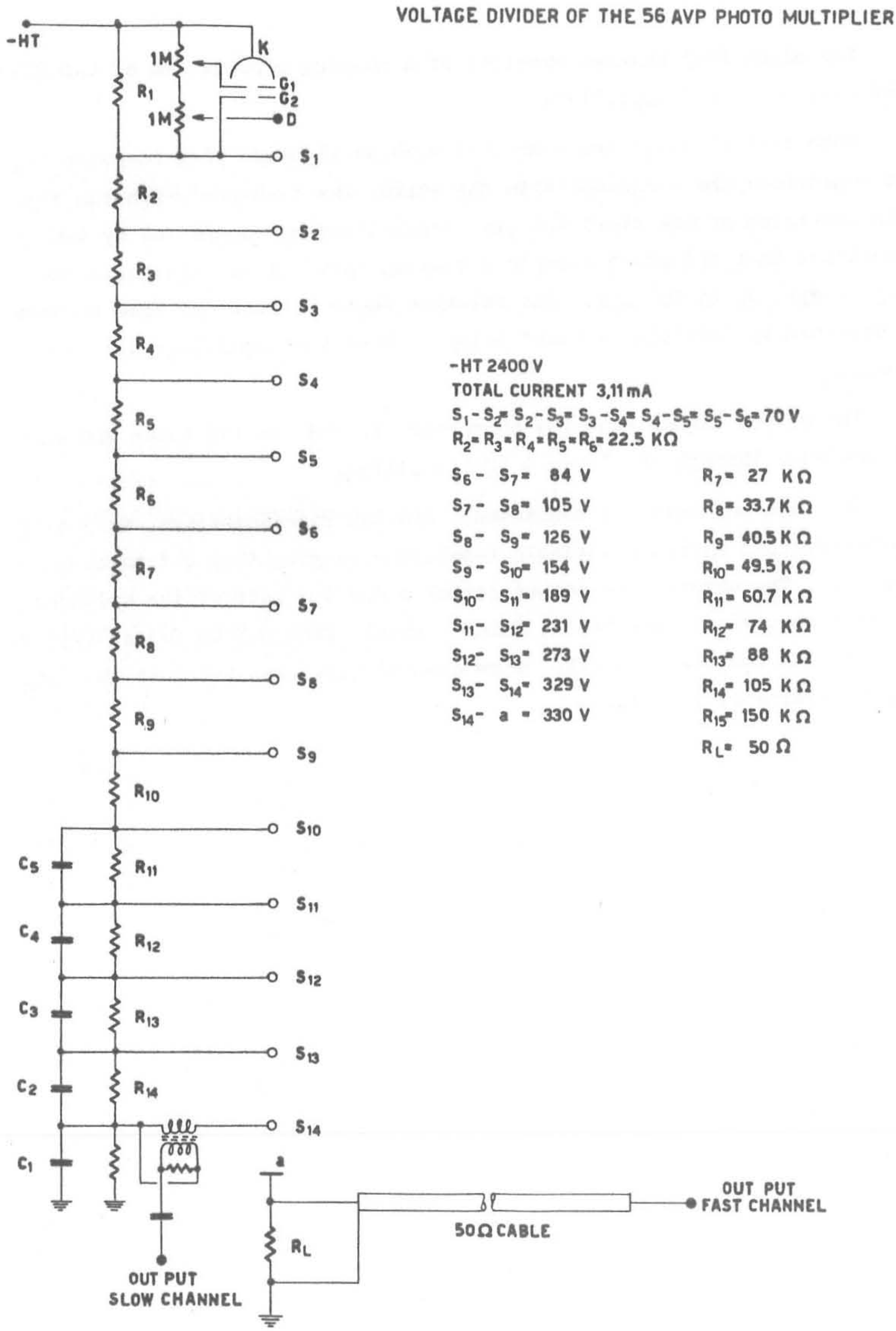
VOLTAGE DIVIDER OF THE 56 AVP PHOTO MULTIPLIER
-HT
1M
1M
K
G1
G2
D
R1 R2 R3 R4 R5 R6 R7 R8 R9 R10 R11 R12 R13 R14
S1 S2 S3 S4 S5 S6 S7 S8 S9 S10 S11 S12 S13 S14
C5 C4 C3 C2 C1
a
RL
-HT 2400 V
TOTAL CURRENT 3,11 mA
S1 - S2 = S2 - S3 = S3 - S4 = S4 - S5 = S5 - S6 = 70 V
R2 = R3 = R4 = R5 = R6 = 22.5 KΩ
S6 - S7 = 84 V
S7 - S8 = 105 V
S8 - S9 = 126 V
S9 - S10 = 154 V
S10 - S11 = 189 V
S11 - S12 = 231 V
S12 - S13 = 273 V
S13 - S14 = 329 V
S14 - a = 330 V
R7 = 27 KΩ
R8 = 33.7 KΩ
R9 = 40.5 KΩ
R10 = 49.5 KΩ
R11 = 60.7 KΩ
R12 = 74 KΩ
R13 = 88 KΩ
R14 = 105 KΩ
R15 = 150 KΩ
RL = 50 Ω
50Ω CABLE
OUT PUT
FAST CHANNEL
OUT PUT
SLOW CHANNEL

Fig. 5

The alpha fast channel consists of a shaping circuit and of two Hewlett Packard type B amplifiers.

Both fast channels are connected with an Eldorado time-to-pulse height converter: the n-channel with the start, the α-channel with the stop. This inversion of the start and stop connections was suggested by the circumstance that the start accepts a maximum rate of 600 cps while the stop accepts up to 10^6 cps. The relative shift between the time signals is obtained by inserting a fixed delay between the amplifiers of the α-channel.

The output signal from the converter is fed to the Laben 200 channel analyser through the Laben G 40 C amplifier.

The slow channels are connected, via two discriminators, to a coincidence circuit having a variable resolution ranging from 0.1 to 0.5 μsec (Fig. 6). The coincidence output signal opens the gate of the multichannel analyser, via an electronic delay variable from 0.5 to 5μsec. (Fig.7)

All the components of the slow channel have been built at the Istituto di Fisica di Trieste.

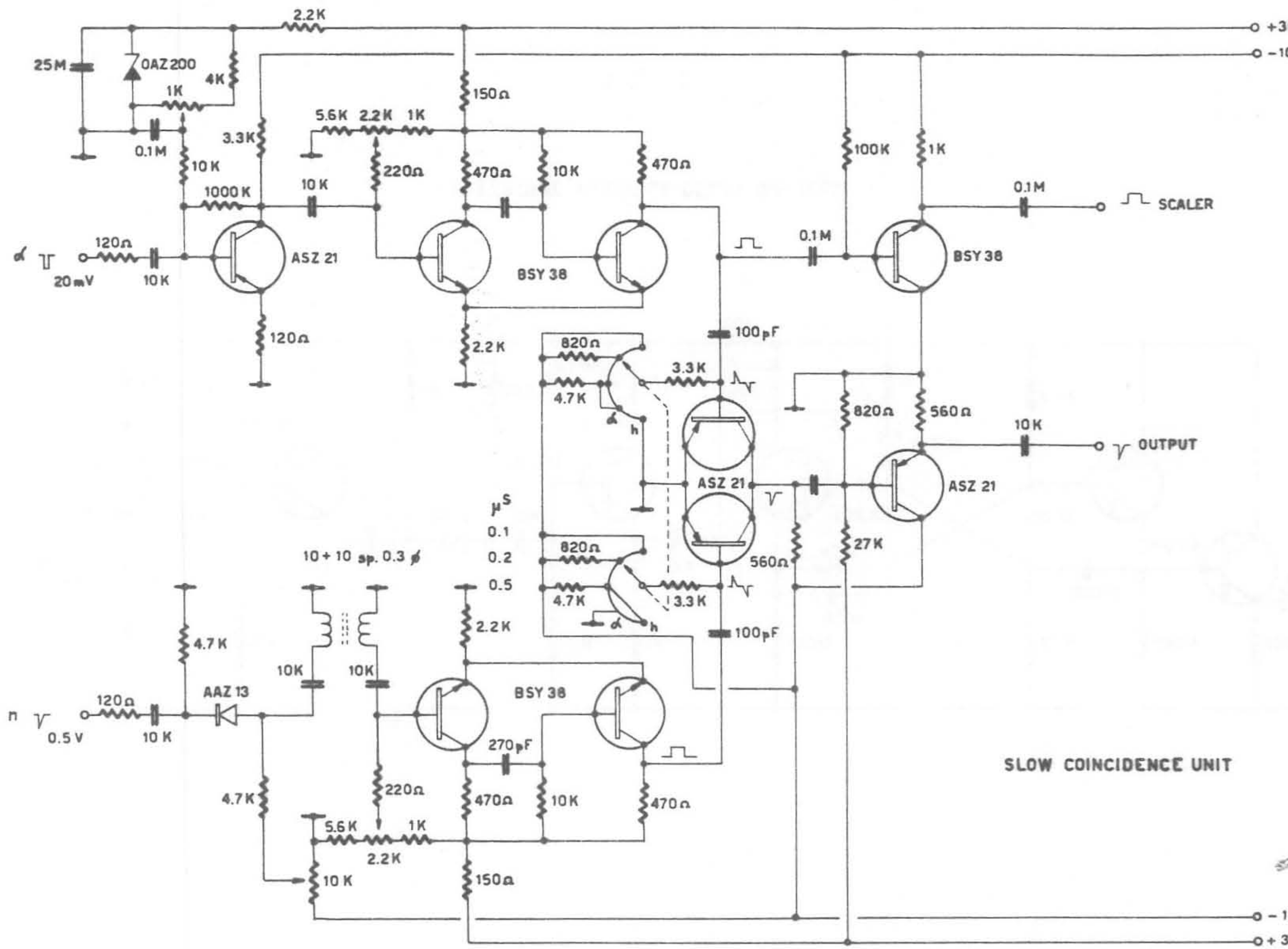
+30
-10
2.2K
25M
0AZ200
4K
1K
0.1M
3.3K
10K
1000K
5.6K
2.2K
1K
150Ω
220Ω
470Ω
10K
470Ω
100K
1K
0.1M
SCALER
120Ω
20mV
10K
ASZ 21
BSY 38
0.1M
BSY 38
120Ω
2.2K
100pF
820Ω
4.7K
3.3K
820Ω
560Ω
10K
OUTPUT
ASZ 21
ASZ 21
μs
0.1
0.2
0.5
10 + 10 sp. 0.3 ø
820Ω
4.7K
3.3K
560Ω
27K
100pF
2.2K
4.7K
10K
10K
AAZ 13
BSY 38
120Ω
0.5V
10K
270pF
4.7K
220Ω
470Ω
10K
470Ω
5.6K
1K
2.2K
10K
150Ω
SLOW COINCIDENCE UNIT
-10
+30

Fig. 6

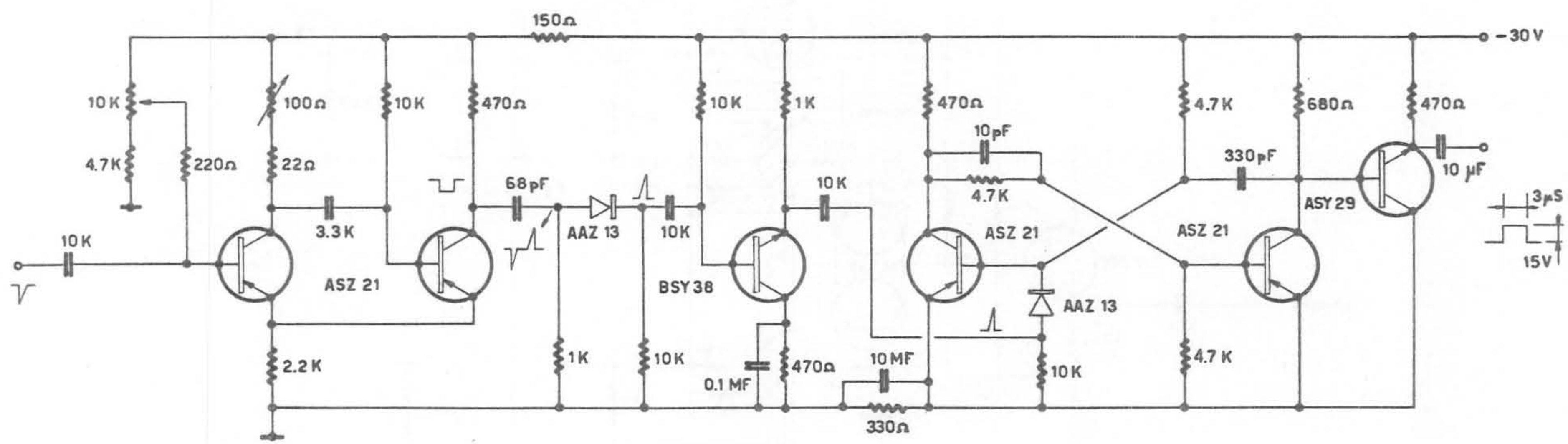

ELETRONIC VARIABLE DELAY 0.5÷6 μS

Fig. 7

3. - THE PULSE SHAPING CIRCUIT

The pulse shaping circuit plays a prominent role and will be therefore described in detail.

The function of the pulse shaping circuit is that of extraction from the pulse delivered by the anode of the phototube a signal to be sent to the time-to-pulse height converter and giving an information concerned with the instant at which a particle has been detected. The shape and amplitude of such signal should be as much constant as possible to make the converter to operate in the proper way.

The principal justification for the use of the pulse shaping circuit is that of obtaining the best time information from the anodic pulse caused by the interaction between the detected particle and the scintillator which consists of processes of intrinsic statistical nature. After Bjerke, ([13]), it has been utilized the central part of the pulse taken from the anode of the phototube since this part is recognized to be the most stable from a statistical point of view ([18]). In fact, on one hand the initial part of the pulse is affected by statistical fluctuations due to the fact that the rather low number of photoelectron emitted by the photocathode makes remarkable both the effect of the random nature of the process of electron emission from the photocathode and the effect connected with the spread of the time intervals, which are needed by the electrons to reach the first dinode and which are different depending upon the point of the photocathode surface from where the electrons originate. On the other hand, the final part of the pulse is altered by several effects among which the ringing and the after pulse effects. ([20])

In order to gain an information from the central part of the pulse, the zero crossing method has been used. ([13]) The bipolar pulse has been obtained by means of an overdamped RLC circuit *). The zero crossing time of the pulse is determined by the operation of a tunnel diode circuit (Fig. 8) which has the characteristics of being very fast and stable.

*) Also a short circuit delay line has been tried, which showed about the same, kind of advantages and disavantages.

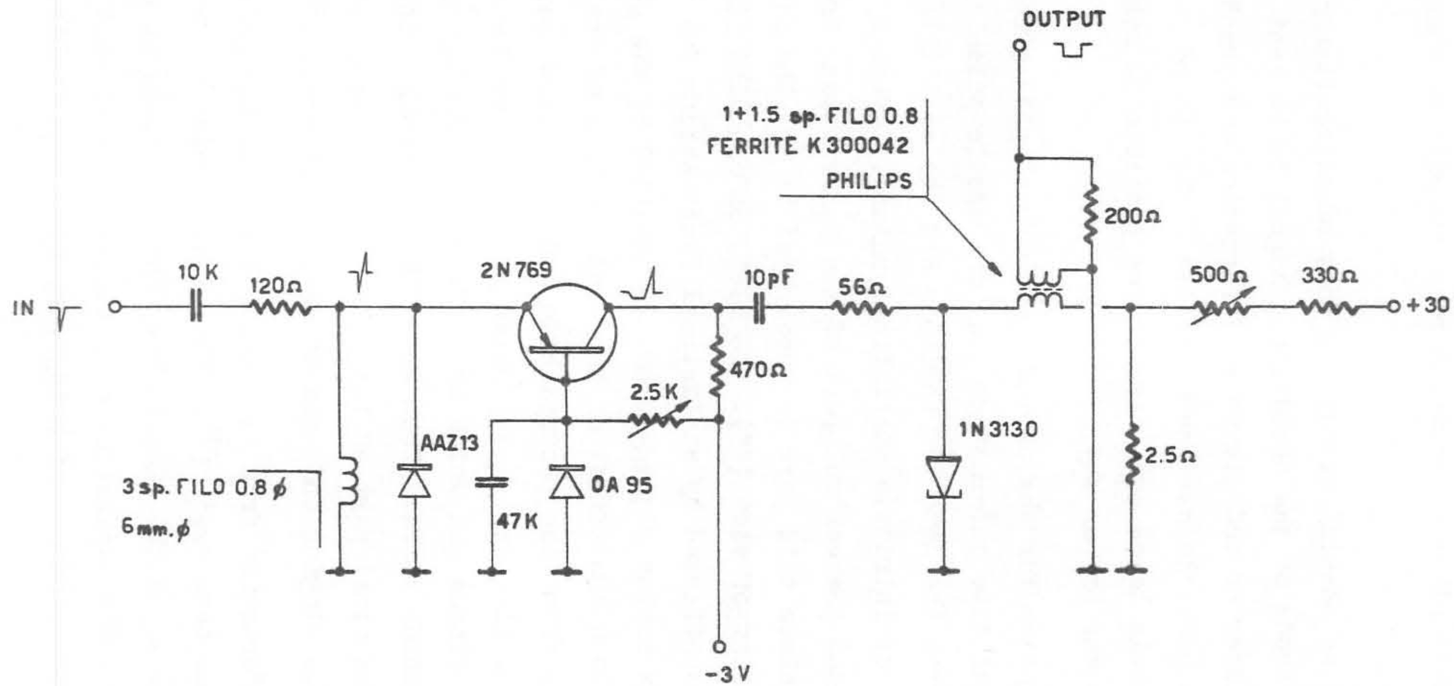

ZERO CROSSING, LIMITING, SHAPING
CIRCUIT WITH TUNNEL DIODE

Fig. 8

4. - RESOLUTION

4.1 Electronic resolution.

The determination of the resolution due to the electronics has been achieved using a mercury relay pulser which simulates coincidence events (Fig. 9). Such tests gave a resolution less than 0.1 ns.

4.2 Resolution measured with the Co^{60} gammas.

By detecting the cascade gammas emitted by a Co^{60} source, the resolution of the whole apparatus, including scintillators, phototubes and electronic circuits, has been tested (Fig.10). In this way one can evaluate with good approximation the contribution to the resolution due to the random nature of the operation of both the scintillator and the photomultiplier. One can also obtain valuable indications concerning the influence of either the dynamic range and the average height of the pulses on the optimization of the operation of the tunnel diode pulse shapers.

Adjusting the slow channel cut-off to allow the transmission of as much a 20% of the dynamic range, a resolution of 1.2 ns has been obtained. This resolution is defined as the width at the half maximum of the coincidence peak.

4.3 Resolution measure with the α-n coincidences.

The above result has been obtained with the pulse shapers set for detecting the α-particles and neutrons and disregarding the γ detection. Therefore, noting that with respect to the pulses due to photons the α particles give smaller pulses and the neutrons five times higher pulses, the test with the Co^{60} gammas was to be expected giving a result worst than that obtained in the test with (α,n) coincidences. In this last case a resolution of 1.40 ns was obtained. This has to be judjed a better resolution than the one obtained with Co^{60}, as the uncertainty introduced by gamma's time flight is relatively negligible. As in case 4.1 the measurement has been performed by analysing the coincidence peak registered by the multichannel analyser.

BLOCK SCHEME OF THE FAST CIRCUIT WITH THE PULSER

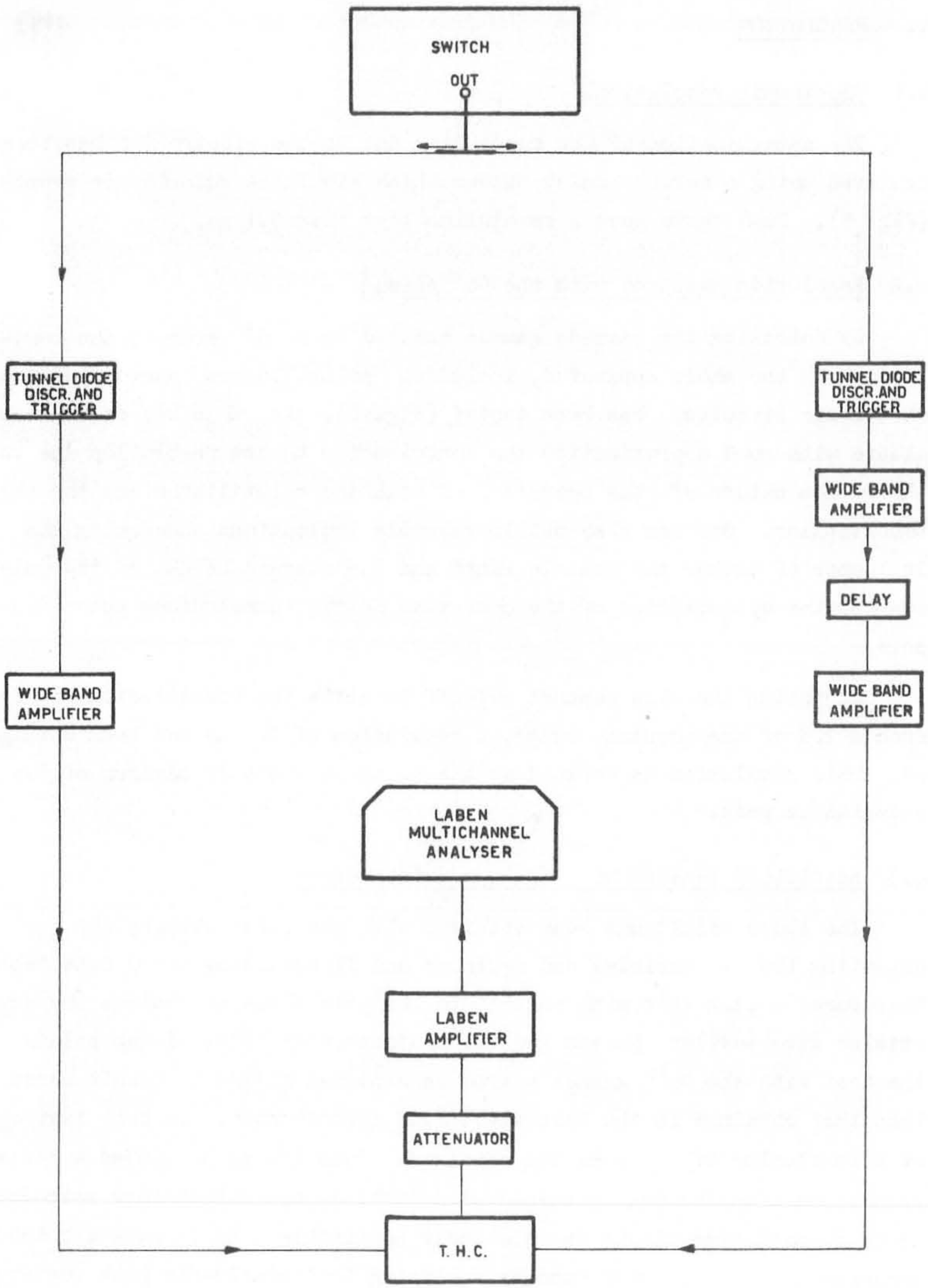

Fig. 9

BLOCK SCHEME WITH Co^{60} γ SOURCE

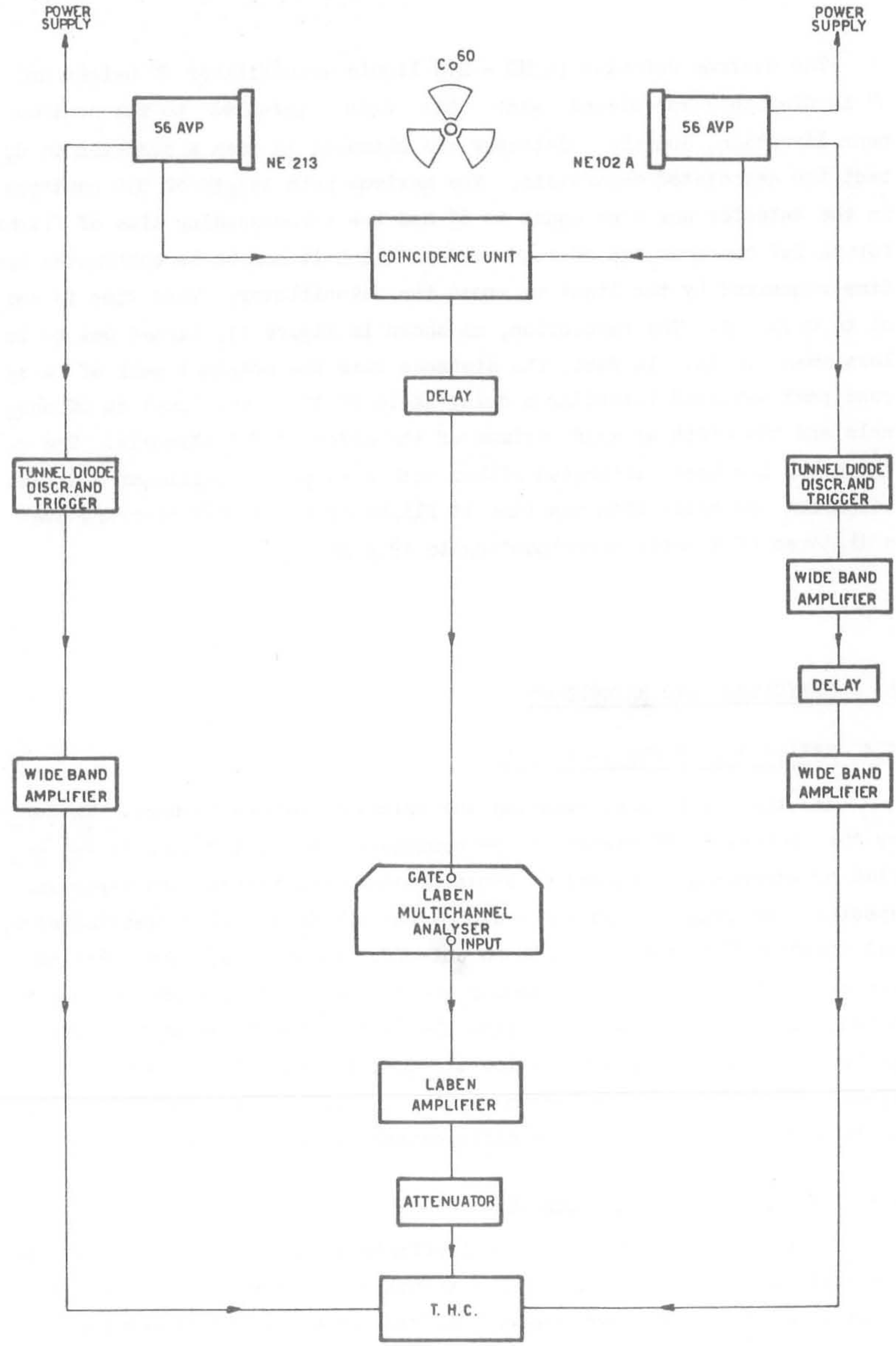

Fig. 10

The neutron detector (a NE - 213 liquid scintillator 3" height and 2" in diameter) was placed with this axis parallel to the neutron beam direction, and the α-detector was situated in such a position to detect the associated α-particle. The maximum path length of the neutrons in the detector was then equal to 3" and the corresponding time of flight for 14 MeV neutrons was of 1.40 ns from which it has to be subtracted the time requested by the light to cross the scintillator. This time is equal to 0.250 ns. The resolution, as shown in Figure 11, turned out to be less than 1.4 ns. In fact, the distance from the original peak of a second peak obtained inserting a delay cable of 10 ns was equal to 60 channels and the width at half maximum of the order of 8.5 channels. The delay cable has been calibrated either with a sampling oscillator and also comparing the delay with the time of flight of the 14 MeV neutrons over a distance of 1 meter corresponding to 19.2 ns.

5. - EFFICIENCY AND BACKGROUND

5.1 Efficiency of the α-channel.

All the α-particles reaching the scintillator are counted. Therefore the detector efficiency can be considered to be 100%, as it is verified by experiment. Figure 12 shows a comparison between two α-particle spectra: spectrum (a), obtained with a cut-off in the slow discriminator, and spectrum (b), obtained with no cut-off. About 3% of the total number of events counted by the scaler are events due to the neutron background or to other reactions, like the (d,d). The first part of the α-particle spectrum, which is below the discriminator thereshold, corresponds to neutrons not belonging to the correlated beam and there fore it does not contribute to the differential cross section.

5.2 Efficiency of the n-channel.

The evaluation of the n-channel efficiency has been carried out particularly in the case of the NE 213 scintillator, used in all the subsequent time of flight measurements, in both parallel and perpendicular

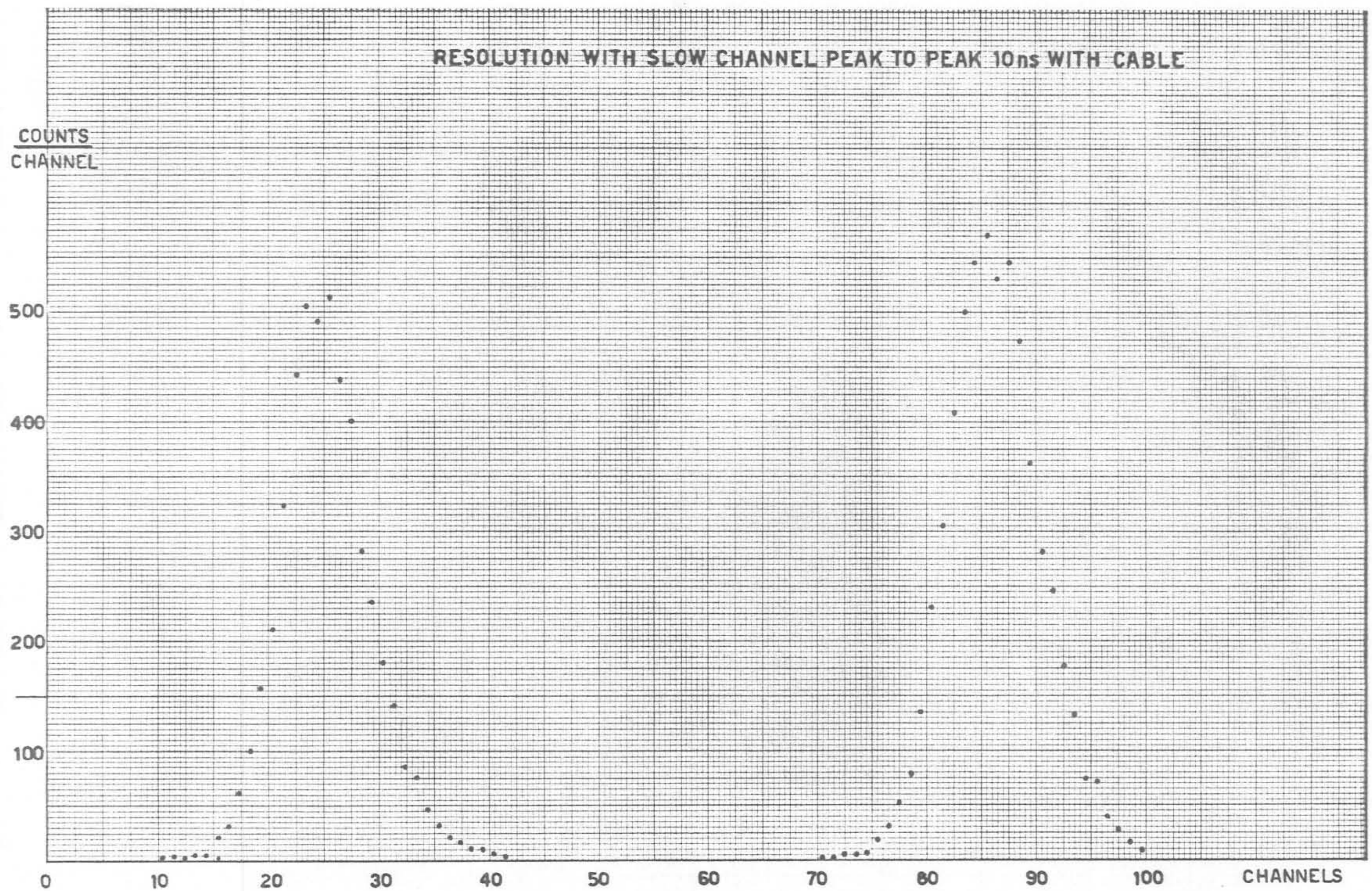
RESOLUTION WITH SLOW CHANNEL PEAK TO PEAK 10ns WITH CABLE
COUNTS
CHANNEL
500
400
300
200
100
0
10
20
30
40
50
60
70
80
90
100
CHANNELS

Fig. 11

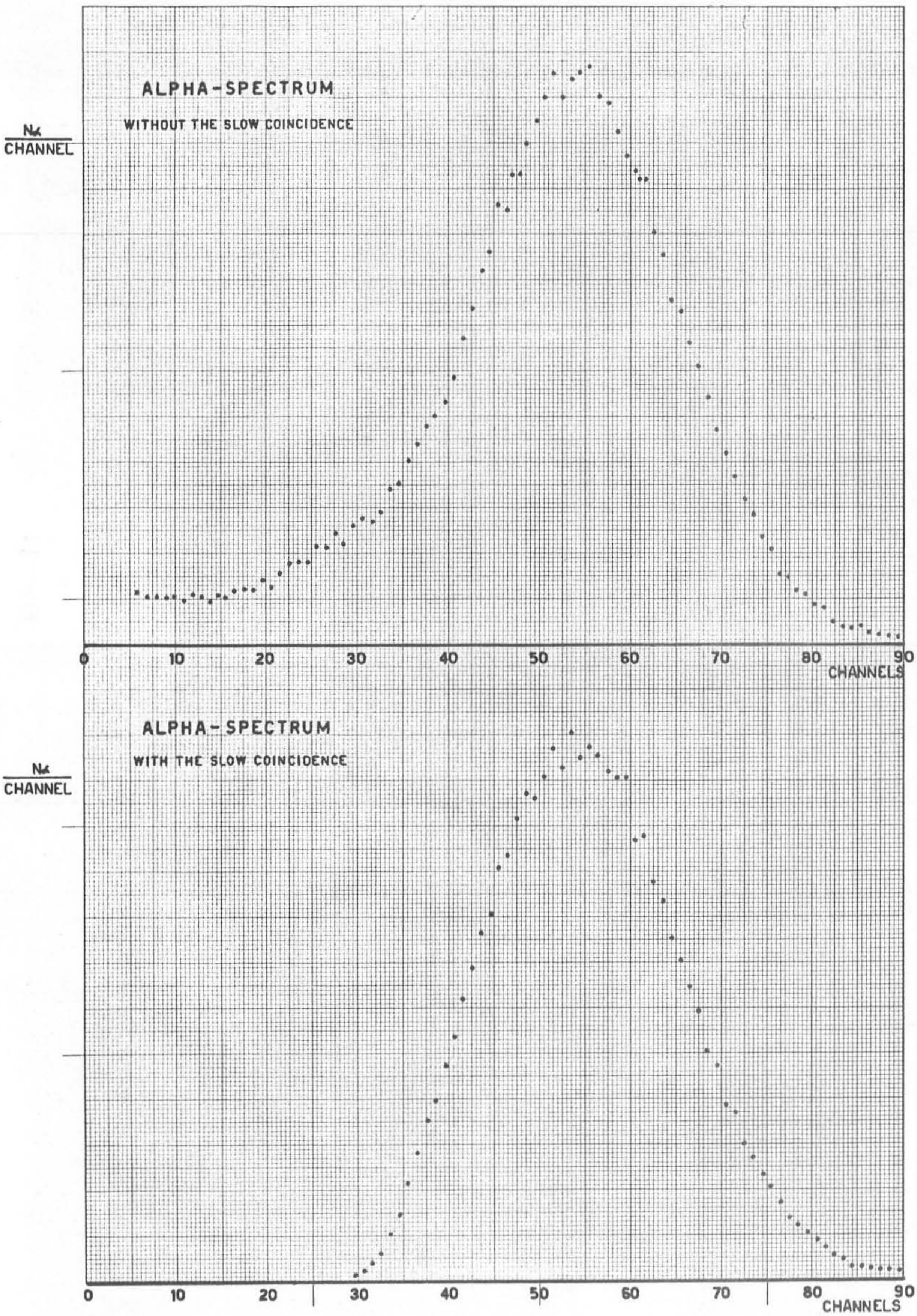
ALPHA-SPECTRUM
WITHOUT THE SLOW COINCIDENCE
Nα / CHANNEL
0
10
20
30
40
50
60
70
80
90
CHANNELS
ALPHA-SPECTRUM
WITH THE SLOW COINCIDENCE
Nα / CHANNEL
0
10
20
30
40
50
60
70
80
90
CHANNELS

Fig. 12

position with respect to the neutron beam direction.

Several theoretical schemes have been considered in order to calculate the detector efficiency for different neutron energies and for various biases of the slow channel discriminator. Formula used by Batchelor [21].

$$(5) \qquad 1 - \exp(-n_H \sigma_H d)$$

neglects either the interaction between neutrons and the carbon nuclei and the double scattering events whose importance increases with the increasing of the neutron path within the scintillator. The efficiency calculated using formula (5) was greater than the experimental one.

In better agreement with the experimental data was the efficiency calculated by means of the formula

$$(6) \qquad \frac{n_H \; H}{n_H \sigma_H + n_c \sigma_c} \left\{1 - \exp\left[-\left(n_H \sigma_H + n_c \sigma_c\right) L\right]\right\}$$

reported by Marion-Fowler [22].

Fig. 13 shows both the expressions (5) and (6) for the efficiency as a function of the scintillator length.

For measuring its absolute efficiency, the detector has been situated so that to garantee that all the neutrons associated with the detected α-particles will impinge upon it. In this manner the efficiency for 14.2 MeV neutrons has been found for various bias values of the slow channel. The experimental data have been compared with the calculations performed using the formula of Rjbakov-Sidorov [23], corrected for the attenuation of the neutron beam within the detector. The formula is

$$\left(1 - \frac{B}{E_n}\right) \frac{n_H \sigma_H}{n_H \sigma_H + n_c \sigma_c} \left\{1 - \exp\left[-(n_H \sigma_H + n_c \sigma_c) L\right]\right\}$$

where B is the energy value corresponding to the slow channel bias.

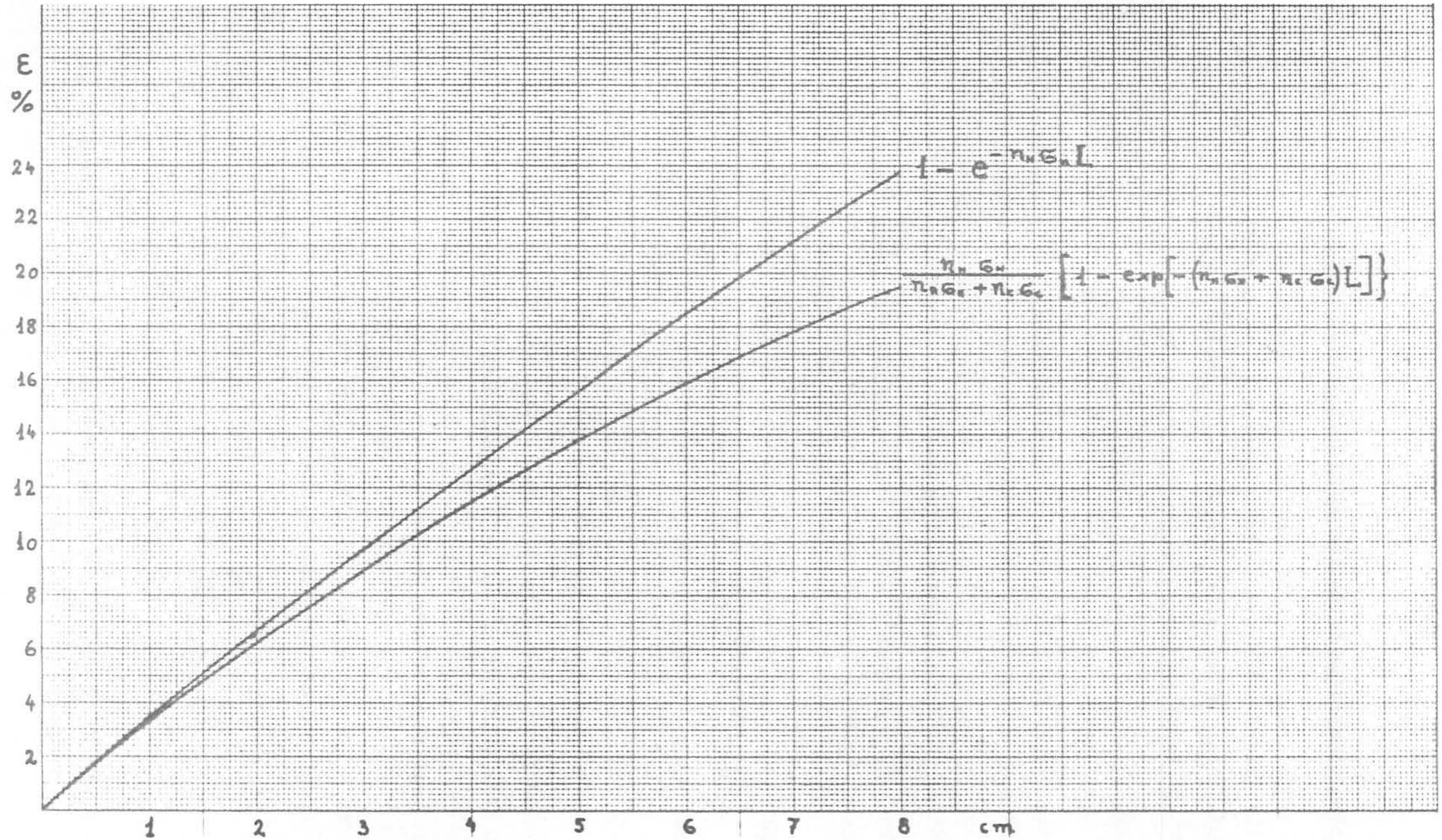

Fig. 13 - Diagrams expressions (5) (6).

It is then clear that the cut-off energy must be very well known.

Since the light quantity emitted by the scintillator does not depend linearly on the energy dissipated by the proton, the Batchelor's formula has been used to get a linear correspondence between the detector response and the energy. Then, using the conversion curves given by Batchelor, a comparison has been made between the data obtained with protons, due to 3 MeV and 14.2 MeV neutrons, and those obtained with Compton electrons knocked out by photons of various energies.

The relative efficiency has been determined using the method of the paraffin scatterer.

5.3 Overall efficiency.

Let the various terms contributing to the overall efficiency be now considered.

The total number of detected neutrons is given by the formula

$$N = N_0 \frac{d\sigma}{d\Omega} \Delta\Omega \frac{\delta}{A} \mathcal{N} L \Sigma_B K(\varphi) . \qquad (8)$$

The various symbol stand for the following quantities. N_0 is the number of neutrons incident upon the sample and is equal to the number of the associated α-particles counted by the α-detector.

$\frac{d\sigma}{d\Omega}$ is the unknown cross-section.

$\Delta\Omega$ is the solid angle from the neutron detector to the sample; in the case of a sample-to-detector distance of 2 meters and using the NE 213 scintillator of 2" diameter one has

$$\Delta\Omega = \frac{S^2}{L^2} = \frac{(2.54)^2\pi}{(200)^2} = 5.06\times10^{-4} \text{ sterad.} \qquad (9)$$

$\frac{\delta}{A} \mathcal{N}$, where the symbols have the usual meaning, gives the number of nuclei per cubic centimeter in the sample.

L is the sample thickness along the direction of the neutron beam.

Σ_B is the detector efficiency corresponding to the thereshold bias B (in MeV) of the slow channel; in the actual experimental conditions Σ_B is of the order of 10^{-7} for one incidente neutron.

$K(\varphi)$ is a correction factor related to the finite dimensions of the sample in a rather complicated manner; it has to be calculated each time the scattering angle φ is changed. Let us consider a neutron interacting with the sample at a depth x (Fig. 14) and scattered at an angle $\varphi < \varphi_{max}$. This neutron has a probability to reach the point x, without interacting with the sample, given by

$$(10) \qquad \exp\left(-\frac{\delta}{A} N \sigma_0 x\right)$$

and has a probability of exit from the sample in the direction φ given by

$$(11) \qquad \exp\left(-\frac{\delta}{A} \mathcal{N} \sigma_e \frac{L - x}{\cos\varphi}\right)$$

Hence, the total probability for the neutron to be detected is

$$(12) \qquad \frac{N}{N_0} = \frac{d\sigma}{d\Omega} \Delta\Omega \, \frac{\delta}{A} \mathcal{N} \Sigma_B \int_0^L \exp\left(-\frac{\delta}{A}\mathcal{N}\sigma_0 x\right) \exp \times$$

$$\times \left(-\frac{\delta}{A}\mathcal{N}\sigma_e \frac{L-x}{\cos\varphi}\right) dx$$

that is

$$(13) \qquad \frac{N}{N_0} = \frac{d\sigma}{d\Omega} \Delta\Omega \, \Sigma_B \frac{\delta}{A} \mathcal{N} L \quad \times$$

$$\times \frac{\exp\left(-\frac{\delta}{A}\mathcal{N} L \frac{\sigma_e}{\cos\varphi}\right) - \exp\left(-\frac{\delta}{A}\mathcal{N} L \sigma_0\right)}{\left(\sigma_0 \frac{\sigma_e}{\cos\varphi}\right) \frac{\delta}{A} \mathcal{N} L}$$

Therefore the correction factor has the expression

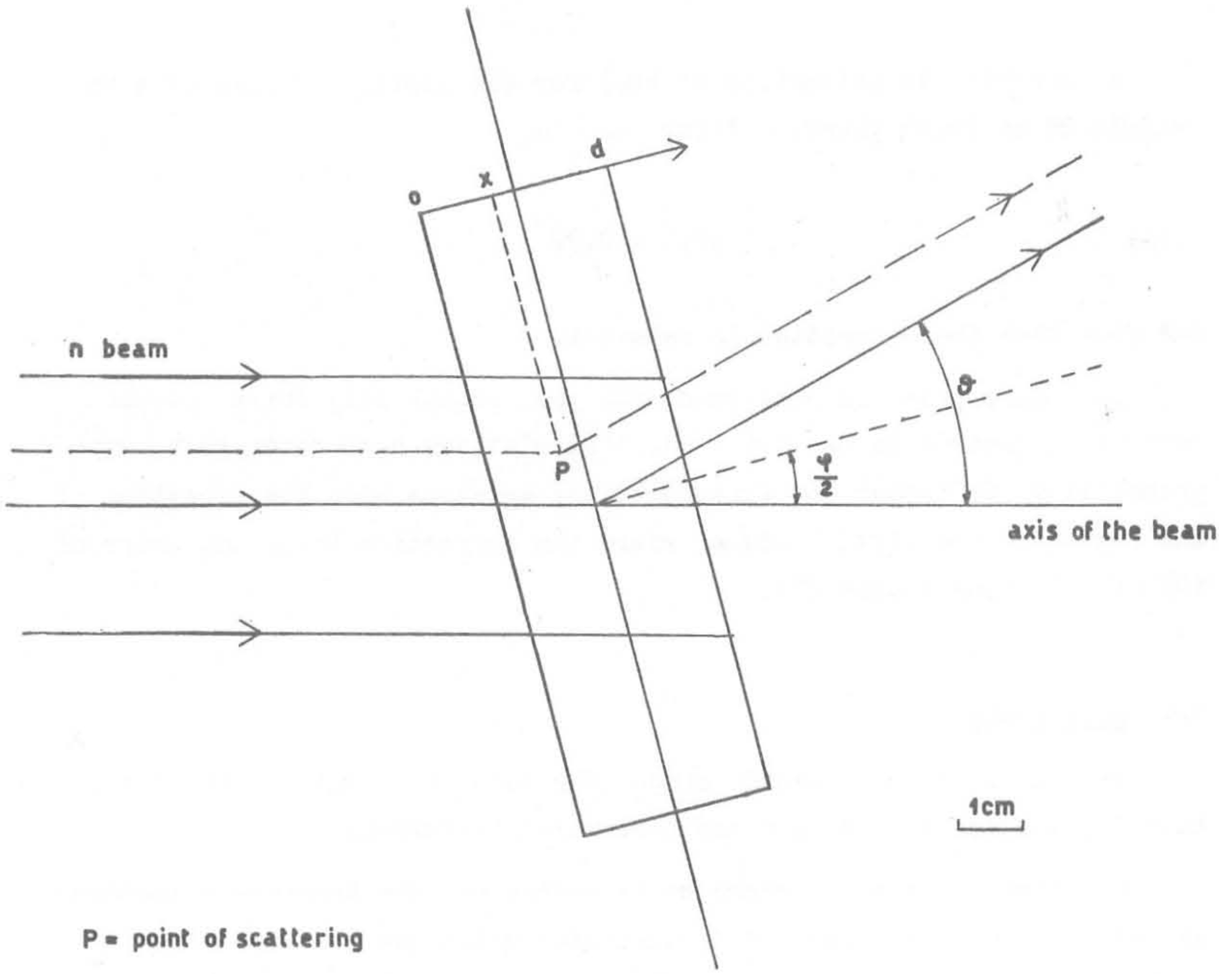

Fig. 14 - Diffusor geometrical scheme.

$$(14) \qquad K(\varphi) = \frac{\exp\left(-\frac{\delta}{A}\mathcal{N} L \frac{\sigma_e}{\cos\varphi}\right) - \exp\left(-\frac{\delta}{A}\mathcal{N} L \sigma_o\right)}{\left(\sigma_o - \frac{\sigma_e}{\cos\varphi}\right)\frac{\delta}{A}\mathcal{N} L}$$

A quantitative estimation of $K(\varphi)$ for the particular case of a Si sample 28 mm thick gives, putting $\sigma_o = \sigma_e$

$$(15) \qquad K(\varphi) = 0.92$$

and show that the correction is relevant.

One more point is concerned with the probability for a double scattered neutron to be detected. Calculations have shown that such probability is rather low throughout the spectrum with the exception of the region of the first minimum, where the correction is of the order of 10% of the true events [24].

5.4 Background.

Two kinds of background affect the time of flight measurements, that is, the correlated and non-correlated background.

The first type of background is caused by the spurious coincidence pulses due to neutrons and α-particles which are not kinematically correlated. To appreciate quantitatively the level of this background in the case of an unshielded detector, one can say that the number of uncorrelated neutrons impinging upon the detector, N_n, depends on the total number of neutrons emitted by the source, N_o, and on a rather complicated factor, Kg, due to the enviromental geometry. One may write

$$(16) \qquad N_n = N_o K_g \quad .$$

On the other hand, the number of true events, N_b, can be expressed by

$$(17) \qquad N_b = N_\alpha K_s$$

where

(18) $$N_\alpha = N_0 \frac{\Omega_\alpha}{4\pi} ,$$

and therefore

(19) $$N_b = N_0 \frac{\Omega_\alpha}{4\pi} K_s .$$

The number of spurious events is given by

(20) $$N_{sp} = N_\alpha \; N_n \; \tau = N_0^{2} \tau \frac{\Omega_\alpha}{4\pi} K_g$$

where τ represents the width of a peak in units of time.

Then, the ratio between spurious and true events is, from (19)and (20),

(21) $$\frac{N_{sp}}{N_b} = \frac{K_g}{K_s} \tau N_0 .$$

In order to reduce the ratio (21) one can diminuish either N_0 or K_g. As far as N_0 is concerned, one can see from Eq. (19) that a reduction of N_0 causes a reduction in N_b. This can be avoided by optimizing K_s and increasing Ω_α, both of which are related in a not simple manner to the overall resolution, since K_s influences the time resolution and Ω_α the angular resolution.

The second type of background is caused by those neutrons associated with the detected α-particles which impinge upon the detector after having been scattered by the laboratory walls. This type of background depends linearly in the number of α-particles detected per sec and therefore the only way to diminuish it consists in limiting the unwanted scattering agents present in the laboratory.

As can be seen from Eq. (21) one has to modify the factor Kg referring to the enviromental geometry.

When the dimensions of the experimental room are small, both types of background are likely to contribute rather largely, particularly if the measurements are made using an unshielded detector. In such conditions it is worthwhile to conveniently shield the detector. Figure 15

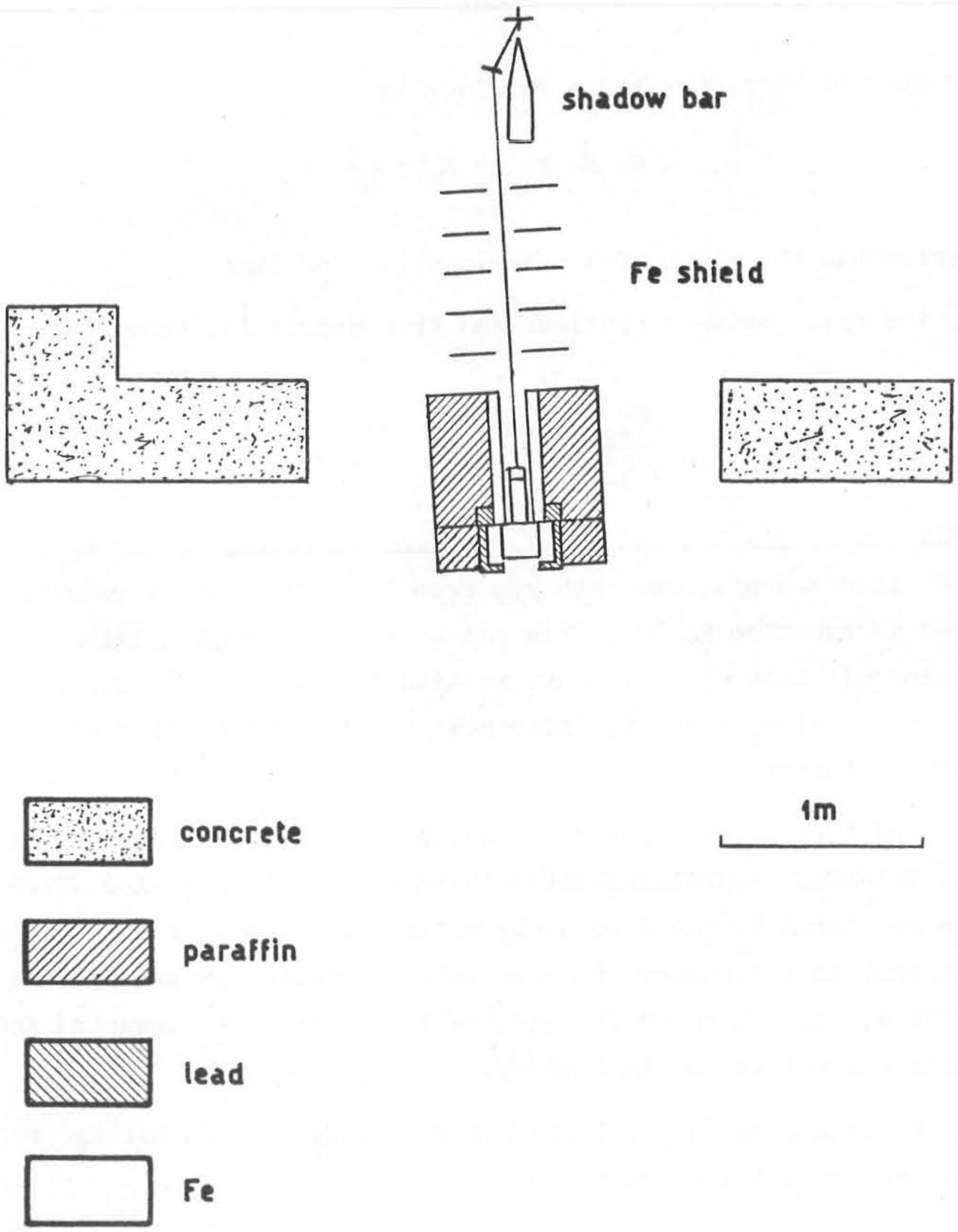

Fig. 15 - Shielding assembly.

shows the shield built at the Istituto di Fisica di Trieste. It consists of an iron, tube, lead rings and bricks, all surrended by paraffin and water tanks. In front of the shield are five iron collimators, 4 cm thick. In this manner, the laboratory background has been eliminated almost completely, but other background sources have been introduced. In fact, the heavy materials of the sield have a neutron scattering cross-sections rather pronunced in the forward direction and this creates a new source of n and γ background. The neutron background was taken into account by normalizing all the measurements with respect to carbon spectra. The gamma background was eliminated by the slow channel bias setting.

An analysis has been carried out to determine the importance of the typer of background mentioned above by measuring the correlated beam without sample and for various angles. It has been found that the magnitude of the noncorrelate background was in agreement with that calculated on the basis of the counting rate in both the n and α channels. On the other hand, the correlate background was almost negligible.

When the sample is on the neutron beam, further source of correlated neutrons is created, which contributes slightly to the correlated background. These are neutrons coming from the sample and scattered into the detector, for example by the shield. This background has been evaluated by comparing the peaks of the direct beam neutrons with those of the neutrons scattered by a Carbon sample.

By virtue of the fact that the elastic peak and the inelastic one in the n-C^{12} diffusion are rather well separated, one can evaluate the background level and the effects on the peak shape as due to the target characteristics and the existing heavy shield.

6. - Experimental results.

The time of flight spectra obtained with three different samples are reported in Figures 16 and 17.

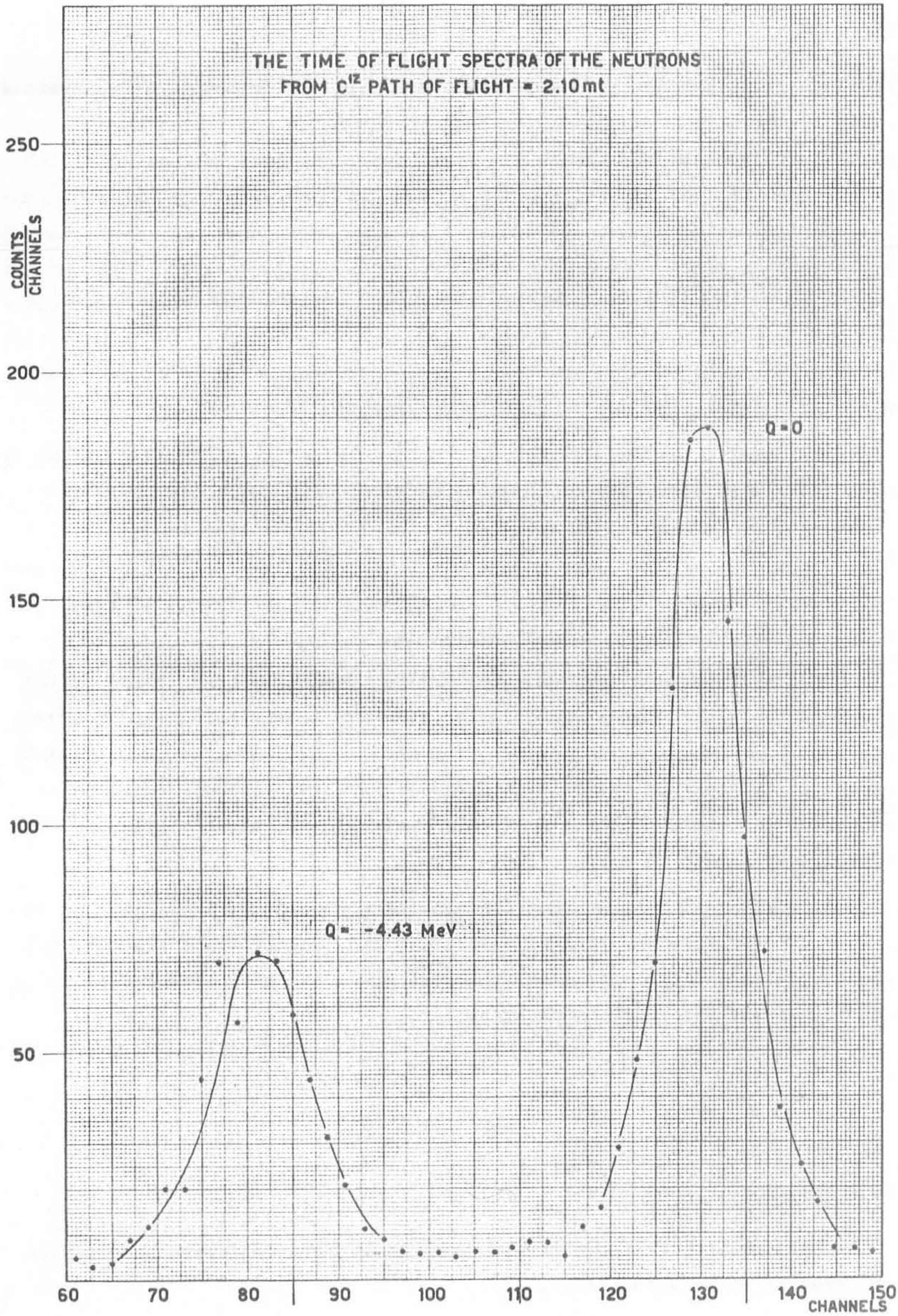
THE TIME OF FLIGHT SPECTRA OF THE NEUTRONS
FROM C^{12} PATH OF FLIGHT = 2.10 mt
COUNTS / CHANNELS
250
200
150
100
50
Q = 0
Q = -4.43 MeV
60
70
80
90
100
110
120
130
140
150
CHANNELS

Fig. 16

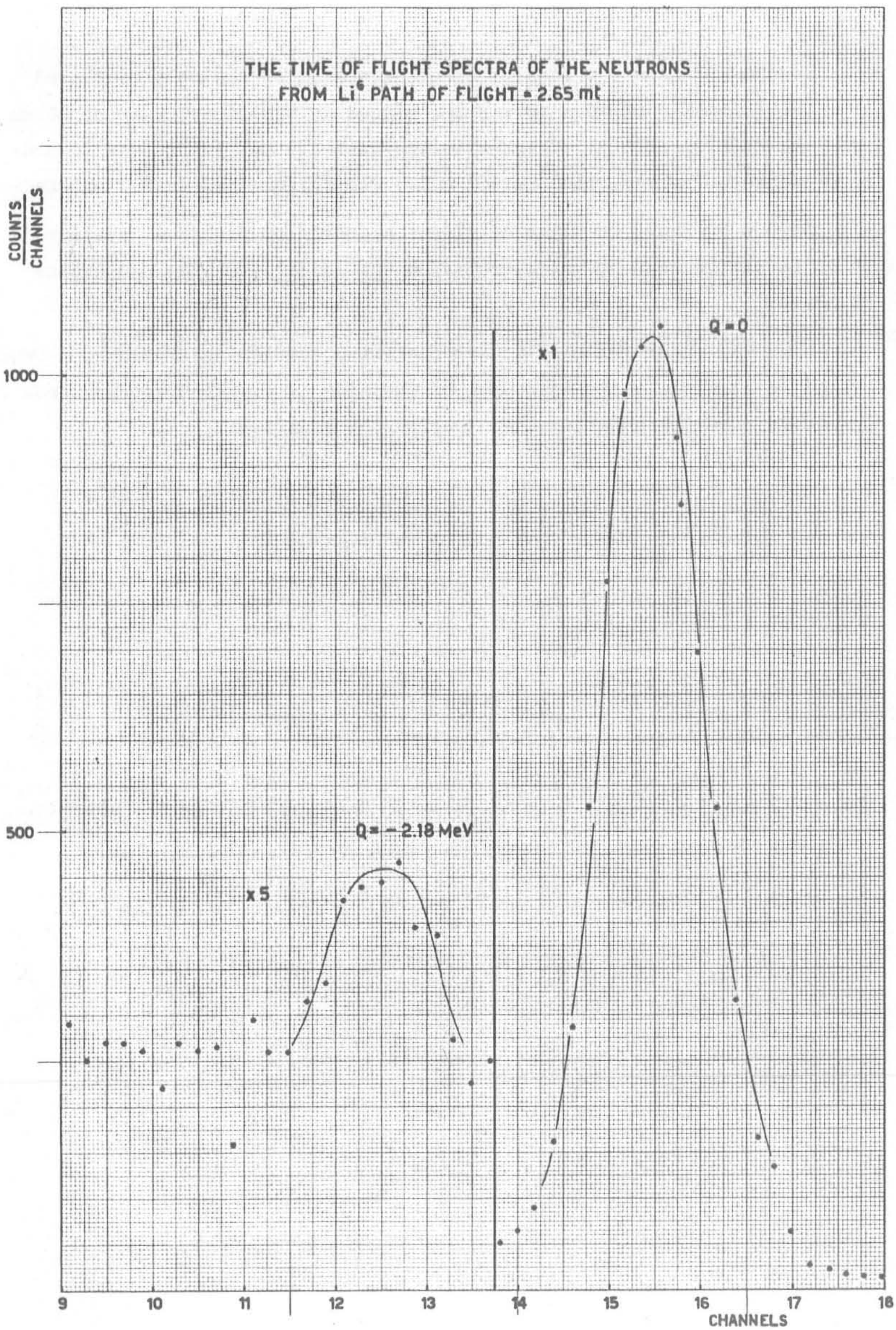
THE TIME OF FLIGHT SPECTRA OF THE NEUTRONS
FROM Li^6 PATH OF FLIGHT = 2.65 mt
COUNTS / CHANNELS
1000
500
Q = 0
x 1
Q = − 2.18 MeV
x 5
9
10
11
12
13
14
15
16
17
18
CHANNELS

Fig. 17

Figure 16 shows the time of flight spectrum of neutrons scattered by a Carbon sample of 10 × 10 × 3 cm, placed in the direct beam at 20 cm from the neutron source. The scattering angle is 46° 30' in the laboratory reference system, that is 50° C.M. The flight path is 2.2 meters.

Figure 17 shows the time of flight spectrum of neutrons scattered by a ^{6}Li sample, 4.5 cm Thick, obtained in still the same conditions as above.

Normally, when the elastic and inelastic scattering of neutrons from nuclei is studied, the measurement of the time of flight spectrum from Carhon is used for checking the experimental apparatus.

REFERENCES

(1) C.F. Cook, Nucl. Instr. and Meth. 15, 137 (1962)

(2) P. Huber, Z. Lewandowski, R. Plattner, C. Poppelbaum and R. Wagner Nucl. Instr. and Meth. 14, 131 (1961)

(3) G.C. Bonazzola and E. Chiavassa, Nucl. Instr. and Meth. 27, 41 (1964)

(4) Garg, Nucl. Instr. and Meth. 6, 72 (1959)

(5) J. Rethmeier, C.C. Jonker, M. Rodenburg, J.W. Hovenier and D.R. Van der Meulen, Nucl. Instr. and Meth. 17, 273 (1962)

(6) G.C. Neilson and D.B. James, Rev. Sci. Instr. 26, 1018 (1955)

(7) I. Szabo, C.E.A. R 2407

(8) P. Perrin, C.E.A. R 2382

(9) P.W. Martin, D.T. Stewart and J. Martin, Nucl. Phys. 61, 524 (1965)

(10) R. Giacomich, F.de Guarrini, G. Pauli and G. Poiani, INFN/BE-66/13

(11) R.L. Clarke, W.G. Cross, Nucl. Phys. 53,177 (1964)

(12) G.C. Bonazzola and E. Chiavassa, Acc. delle scienze

(13) A.E. Bjerke, Q.A. Kerns, T.A. Nunamaker, Nucl. Instr. and Meth. 15, 249 (1962)

(14) J. Garvey, Nucl. Instr. and Meth. 29, 137 (1964)

(15) R. Van Zurk, C.E.A. R 2405

(16) R. Van Zurk, Nucl. Instr. and Meth. 16, 157 (1962)

(17) D.L. Wieber, Nucl. Instr. and Meth. 24, 269 (1963)

(18) M. Hesse, C.E.A. R 2382

(19) Y. Koechlin, Thesis, Paris (1961) C.E.A. R 2194

(20) J.B. Birks, The theory and pratice of scintillation counting, Oxford Pergman Press, 1964, chapt. 5

(21) R. Batchelor, W.B. Gibboy, J.B. Parker, J.H. Towle,
Nucl. Instr. and Meth. 13, 70 (1961)

(22) J.B. Marion, J.L. Fowler, Fast Neutron Physics, Vol. IV -part I
Interscience Publishers, Inc. New York

(24) B.V. Rybakov, V.A. Sidorov, Fast Neutron Spectroscopy, Consultants
Bureau, Inc., New York

* * *